COBEM 2023 27TH INTERNATIONAL CONGRESS OF MECHANICAL ENGENEERING

ABCM Brazilian Society of Mechanical Sciences and Engineering
27th ABCM International Congress of Mechanical Engineering
December 04-08, 2023, Florianópolis-SC, Brazil

COB-2023-0147
Effects of Rational-Function Approximation Coefficients on the Aeroelastic Analysis of Transonic Flutter with CFD-Based Reduced-Order Model

Ana Cristina Neves Carloni
Instituto Tecnológico de Aeronáutica, 12228-900 São José dos Campos, SP, Brazil
ana.nevescarloni@gmail.com

João Luiz F. Azevedo
Instituto de Aeronáutica e Espaço, 12228-904 São José dos Campos, SP, Brazil
joaoluiz.azevedo@gmail.com

Abstract. *The current work is concerned with studying the effects of rational-function approximation (RFA) coefficients used to represent the unsteady aerodynamics based on computational fluid dynamics (CFD) results on the transonic aeroelastic stability analyses. The CFD calculations are based on the Euler equations, and the code uses a finite volume formulation for general unstructured grids. A centered spatial discretization with added artificial dissipation is used, and an explicit Runge-Kutta time marching method is employed. The dynamic system considered in the present work is a NACA 0012 airfoil-based typical section in the transonic regime. Unsteady calculations are performed for mode-by-mode and simultaneous excitation approaches, the latter defined by orthogonal Walsh functions. A technique based on power spectral density (PSD) is employed to allow the splitting of the aerodynamic coefficient time histories into the contribution of each individual mode to the corresponding aerodynamic transfer functions. Generalized unsteady aerodynamic forces are approximated by a rational function in the Laplace domain, in which nonlinear parameters are selected through a non-gradient optimization process. Results indicate that small variations in the aerodynamic lag states that compose the rational-function approximation considerably impact the flutter onset point identification in frequency-domain aeroelastic stability analyses.*

Keywords: *Rational-Function Approximation, Reduced-Order Model, Flutter, Aeroelasticity*

1. INTRODUCTION

In the past decades, traditional aeroelastic analysis implements an explicit coupling of aerodynamic and dynamic-structural systems by carrying out an interactive process (Silva *et al.*, 2009). Accordingly, parametric and flight condition variations necessarily demand a repetitive use of high-fidelity CFD codes in unsteady mode. Given the available computational power, the traditional aeroelastic approach is impractical for engineering applications that require an extensive sweep over the entire flight envelope. Even nowadays, aircraft designs with large aspect ratio, flexibility, and complexity usually compromise traditional aeroelastic analysis feasibility. As a consequence, this impacts the structural stability condition mapping, which is critical for preventing the occurrence of aeroelastic phenomena such as flutter (Bisplinghoff *et al.*, 1955). One of the most prominent approaches to tackle this challenge is the reduced-order model (ROM) formulation, where the prevailing dynamics of the aerodynamic system is captured. In essence, the objective of the present work is to improve the procedure developed to analyze transonic aeroelastic phenomena using reduced-order models by investigating the impact of the nonlinear rational-function approximation (RFA) coefficients on the results of frequency-domain aeroelastic stability analyses.

The CFD code used here is based on the 2-D Euler equations, which are discretized using a finite volume approach for unstructured grids. A centered scheme with added artificial dissipation is used for spatial discretization and explicit Runge-Kutta methods are employed for time marching. The present paper concentrates initially on identifying the aerodynamic transfer functions from a unique excitation in all the natural modes of the typical section model. This identification procedure is based on the computation of power spectral densities of the inputs and outputs of the dynamic system. Once the transfer functions are obtained, they can be represented by a rational-function approximation in the Laplace domain in order to better suit the solution of the aeroelastic eigenvalue problem (Eversman and Tewari, 1991). Finally, the solution of such eigenvalue problem for varying dynamic pressures yields a root locus from which one can estimate the flutter boundary of the configuration.

2. THEORETICAL FORMULATION

2.1 General Formulation

The structural model considered in the present work is the typical section, which is widely known and reported in literature (Bisplinghoff *et al.*, 1955; Azevedo *et al.*, 2013). The dynamic system represented in the typical section is a rigid airfoil with two degrees of freedom, namely plunge and pitch. Figure 1 presents a typical section configuration scheme, where h is the vertical translation, positive downwards, and α is the pitch mode coordinate, positive in the nose-up direction. In addition, c is the airfoil chord, b is the semi-chord length, x_α is the distance from the elastic axis to the center of mass normalized by the semi-chord, a_h is the distance from mid-chord to the elastic axis normalized by the semi-chord, and k_h and k_α are the stiffness coefficients associated with plunge and pitch modes, respectively.

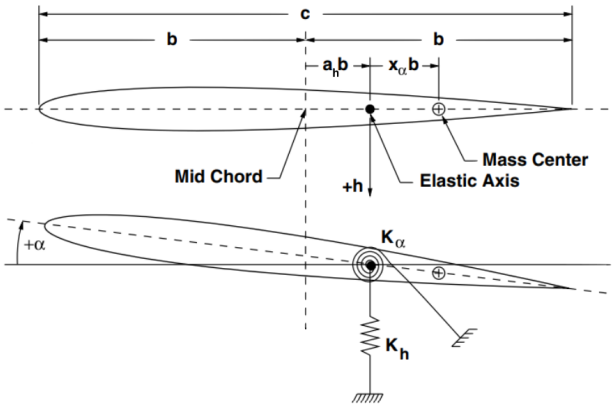

Figure 1. Typical section configuration adapted from Thomas and Dowell (2019).

The mesh used in the present work, shown in Fig. 2, is the same previously investigated and used by Azevedo *et al.* (2013). It was generated with the commercial grid generator ICEM CFD©, and has about 16,000 triangular control volumes and just over 290 points along the airfoil. The adopted mesh movement takes into account the body motions involved in unsteady calculations by rigidly moving the mesh accordingly, without volume deformations. In this approach, the far-field boundary conditions are adjusted to account for the boundary movement with the rest of the mesh.

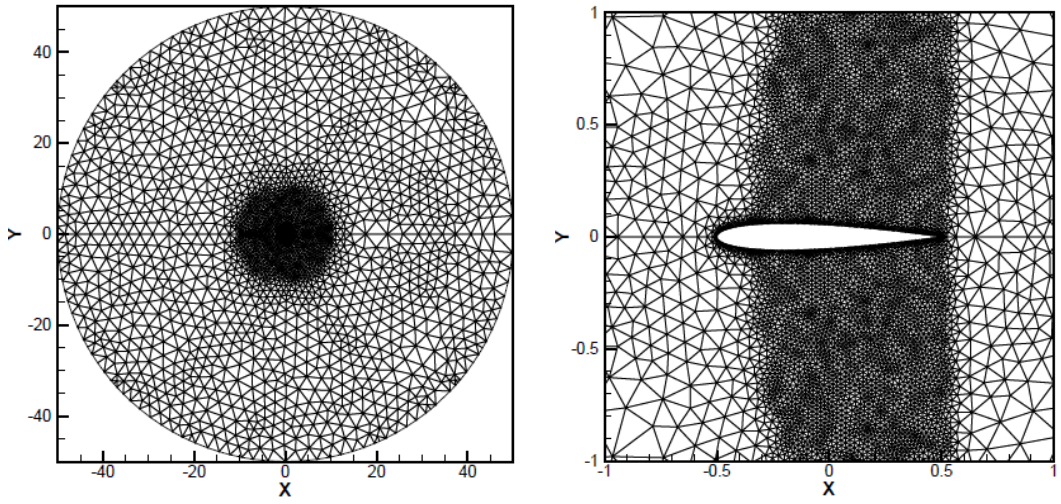

(a) Complete mesh with 8,323 nodes and 16,232 volumes. (b) Mesh view around the NACA 0012 airfoil.

Figure 2. Mesh around NACA 0012 profile with 50 chord-lengths of distance between the body and the far-field and 292 wall points. Taken from Marques and Azevedo (2008).

A general aeroelastic system is characterized by aerodynamic, elastic and inertial forces dynamically interacting with structural deformations (Bisplinghoff *et al.*, 1955). It is very common to represent the aerodynamic effects exclusively through the resulting forces and moments acting on the structure as a forcing term in the dynamic equations. As such, the

governing equation for this dynamic system is given by

$$[M]\{\ddot{\eta}(t)\} + [K]\{\eta(t)\} = \{Q_a(t)\}, \tag{1}$$

where $[M]$ and $[K]$ are, respectively, the generalized mass and stiffness matrices, $\{\eta(t)\}$ is the generalized coordinate, and $\{Q_a(t)\}$ represents the generalized aerodynamic forces (GAFs).

As a consequence of linearity assumptions, it is possible to determine the aerodynamic response to a general structural behavior from the convolution of an impulsive or indicial aerodynamic solution (Bisplinghoff *et al.*, 1955). The convolution operation, however, is more easily handled in the frequency domain, in which it is represented by a simple multiplication operation. Hence, the aerodynamic forces due to the structural motion, linearized with regard to the modal displacements, can be written in the reduced frequency domain. After some mathematical manipulations, it is possible to define the generalized aerodynamic forces as

$$\{\bar{Q}_a(\kappa)\} = \frac{(U^*)^2}{\pi\mu}[A(\kappa)]\{\eta(\kappa)\}, \tag{2}$$

where μ is the mass ratio, U^* is the characteristic speed, and the aerodynamic influence coefficient matrix is given by

$$[A(\kappa)] = \begin{bmatrix} -C_{l_h}(\kappa)/2 & -C_{l_\alpha}(\kappa) \\ C_{m_h}(\kappa) & 2C_{m_\alpha}(\kappa) \end{bmatrix}. \tag{3}$$

2.2 SIMO and MIMO Approaches

There are different approaches to determine the aerodynamic coefficients due to each modal motion from unsteady CFD simulations. Assuming small-amplitude motions, one can formulate the transonic aeroelastic problem as a linear dynamic system in the frequency domain. In this case, the linear dynamic system would have the modal motions of the structure as inputs and the unsteady GAFs developed in response to the modal motions as outputs. As a consequence of the linearity assumption, it is possible to determine the aerodynamic response to a general structural behavior from the convolution of an impulsive or indicial aerodynamic solution (Bisplinghoff *et al.*, 1955; Silva and Bartels, 2004). This happens because, in linear systems, the response to a certain modal motion is independent of other modal motions and, hence, it is possible to excite the modes one at a time. This corresponds to the single-input/multiple-output (SIMO) approach. It essentially changes the one multiple-input/multiple-output (MIMO) problem into several SIMO problems.

On the other hand, instead of gathering individual impulse responses due to one input at a time, the MIMO approach proposes to perform a single unsteady CFD simulation where the modal motions are prescribed in order to simultaneously excite all the system modes. For the simultaneous excitation of a MIMO system, system identification techniques dictate that the input functions used to excite the system must be properly defined in order to generate accurate input-output models of the system (Silva, 2018). The most important point to keep in mind when defining these input functions is that these functions and their derivatives need to be somehow uncorrelated. Otherwise, if identical excitation inputs are applied simultaneously, it becomes practically impossible for any system identification algorithm to relate the effects of one input on a given output.

2.3 Orthogonal Walsh Functions

After comparing several orthogonal input signals such as block pulse, Haar, and Walsh functions, Silva (2008) had concluded that orthogonal Walsh functions are well-suited for the identification of CFD-based unsteady aerodynamic ROMs. For this reason, the Walsh functions are selected in this work as the simultaneous orthogonal inputs to prescribe the modal motions of the typical section during the unsteady CFD simulations. This family of functions is similar to conventional step inputs and, therefore, embodies their impulsive nature with regard to frequency bandwidth. More specifically, the Walsh functions are a set of block step functions that form an orthogonal basis of the square-integrable functions (Azevedo *et al.*, 2013). Each function takes positive and negative unitary values, and each step block period is an integer multiple of a 2^n division of the function length. The Walsh function inputs illustrated in Fig. 3 are considered for generating the unsteady aeroelastic results using the MIMO approach presented throughout this work.

2.4 Rational-Function Approximation Formulation

In order to carry out a frequency-domain aeroelastic stability analysis using a continuous-time state-space formulation, it is convenient to somehow adjust the discrete sets of CFD-based aerodynamic responses to the orthogonal Walsh functions. One possible solution is to represent these data using rational-function approximations (RFAs). In essence, the RFA procedure proposes a curve fitting to the aerodynamic responses obtained from CFD calculations. There is a wide number of eligible polynomials reported in the literature (Tiffany and Adams, 1988; Eversman and Tewari, 1991) from which the polynomial proposed by Eversman and Tewari (1991) without any provision for the treatment of repeated,

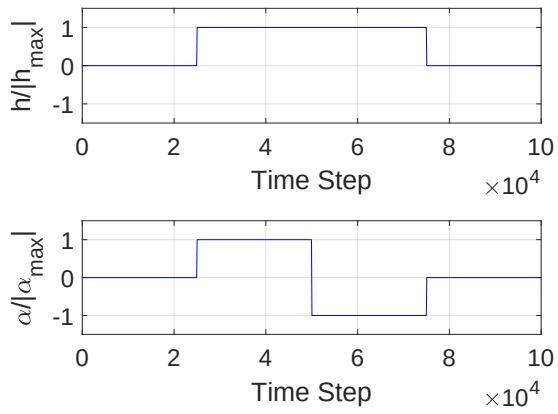

Figure 3. Normalized modal motions prescribed by orthogonal Walsh function inputs.

or very close, poles is initially selected in this work for implementation and tests. This choice is based on the fact that such polynomials are the most commonly used in similar applications and that they are conveniently constructed for the formulation of aerodynamic state variables.

In the Laplace domain, the rational-function approximation referred to as the first form of the Eversman and Tewari interpolating polynomials is written as

$$[A(\bar{s})] = [A_0] + [A_1]\frac{\bar{s}}{U^*} + [A_2]\left(\frac{\bar{s}}{U^*}\right)^2 + \sum_{n=1}^{n_\beta}\left([A_{n+2}]\frac{U^*}{\bar{s}+U^*\beta_n}\right), \tag{4}$$

where the β_n's are the poles that introduce the aerodynamic lags with respect to the structural modes. Moreover, n_β is the total number of poles, and $[A_n]$ are the approximating coefficient matrices. The polynomial coefficients $[A_n]$ and β_n are determined by an optimized least-squares approximation method. In this approach, the numerator coefficients are determined by a least-squares fit, whereas the denominator coefficients are included as the free parameters of a simplex non-gradient optimization process (Nelder and Mead, 1965).

The second form of Eversman and Tewari interpolating polynomials consistently accounts for cases where the optimized values of two or more poles of the approximation are close to one another. Such condition characterizes the phenomenon of repeated poles, which makes the subsequent eigenvalue problem poorly conditioned. To overcome this difficulty, Eversman and Tewari (1991) propose a slight modification to the lag terms in such situations. Simply put, when two poles are very close to each other, Eversman and Tewari (1991) show that these poles can be represented by only one of them. However, this pole with double multiplicity must appear in two terms of the polynomial – one linear and one quadratic. Similarly, this analysis can be extended in the case of three, four, or actually any number of poles that occur very close to each other. To account for poles with multiplicity, the second form of Eversman and Tewari interpolating polynomials is formulated as

$$\begin{aligned}[A(\bar{s})] =& [A_0] + [A_1]\frac{\bar{s}}{U^*} + [A_2]\left(\frac{\bar{s}}{U^*}\right)^2 + \sum_{n=1}^{n_\beta}\left(\left[A_{(n+2)}\right]\frac{U^*}{\bar{s}+U^*\beta_n}\right) \\ &+ \sum_{n=n_{\beta_1}+1}^{n_\beta}\left(\left[A_{(n+N_2+2)}\right]\frac{(U^*)^2}{(\bar{s}+U^*\beta_n)^2}\right) \\ &+ \sum_{n=n_{\beta_2}+1}^{n_\beta}\left(\left[A_{(n+N_3+2)}\right]\frac{(U^*)^3}{(\bar{s}+U^*\beta_n)^3}\right) \\ &+ \sum_{n=n_{\beta_3}+1}^{n_\beta}\left(\left[A_{(n+N_4+2)}\right]\frac{(U^*)^4}{(\bar{s}+U^*\beta_n)^4}\right) + \dots\end{aligned} \tag{5}$$

with

$$N_2 = n_\beta - n_{\beta_1}, \quad N_3 = 2n_\beta - n_{\beta_1} - n_{\beta_2}, \quad N_4 = 3n_\beta - n_{\beta_1} - n_{\beta_2} - n_{\beta_3}, \quad \dots \tag{6}$$

where n_β is the total number of poles, and it is assumed that the $\beta_1, \dots, \beta_{n_{\beta_1}}$ are non-repeated poles, $\beta_{(n_{\beta_1}+1)}, \dots, \beta_{n_{\beta_2}}$ are poles that occur twice, $\beta_{(n_{\beta_2}+1)}, \dots, \beta_{n_{\beta_3}}$ are poles that occur three times, and so on.

3. RESULTS AND DISCUSSION

3.1 Simulation Procedure

The aeroelastic system considered throughout this paper involves a NACA 0012 airfoil at $M_\infty = 0.8$, that is, in the transonic regime, and $\alpha_0 = 0$. The structural parameters that define the system are $a_h = -2.0$, $x_\alpha = 1.8$, $r_\alpha = 1.865$, $\mu = 60$, $\omega_h = \omega_\alpha = 100$ rad/s, and $\omega_r = \omega_\alpha$ is used as a reference. Here, r_α is the airfoil dimensionless radius of gyration about the elastic axis, and ω_h and ω_α are the uncoupled natural circular frequency of the plunge and pitch mode, respectively. A steady-state solution at the mean flow condition is used to initialize all the unsteady CFD runs. Such solution is obtained by the same CFD code running in steady mode with a variable time step method, *i.e.*, constant CFL number.

For the present work, discrete step and Walsh function inputs are considered in order to prescribe the airfoil movement in the unsteady CFD simulations. It is important to emphasize that the discrete step inputs are used in a mode-by-mode fashion, whereas the Walsh functions are used to simultaneously excite all the system modes. Thus, the former refers to the SIMO approach, whereas the latter refers to the MIMO approach. Consequently, the simulations with any set of Walsh functions require only one unsteady CFD run, whereas those with discrete step inputs would require two simulations in the present case, one for each modal movement. Furthermore, the maximum amplitudes of the modal motions are $0.000001c$ for the plunging mode and 0.0001 deg. for the pitching degree of freedom, where c is the airfoil chord length. The main reason for choosing such low amplitudes is to remain within the linear region around the nonlinear steady solution.

3.2 Aerodynamic Transfer Functions

The present work initially concentrates in identifying the aerodynamic transfer functions from a unique excitation in all the natural modes of the typical section. This identification procedure is based on the computation of power spectral densities (PSDs) of the inputs and outputs of the dynamic system. A relatively simple approach to estimate the transfer functions is by a division in the frequency domain for uncorrelated input signals and its derivatives. The validation of the PSD procedure is achieved by comparing the transfer functions obtained based on the MIMO approach with the ones

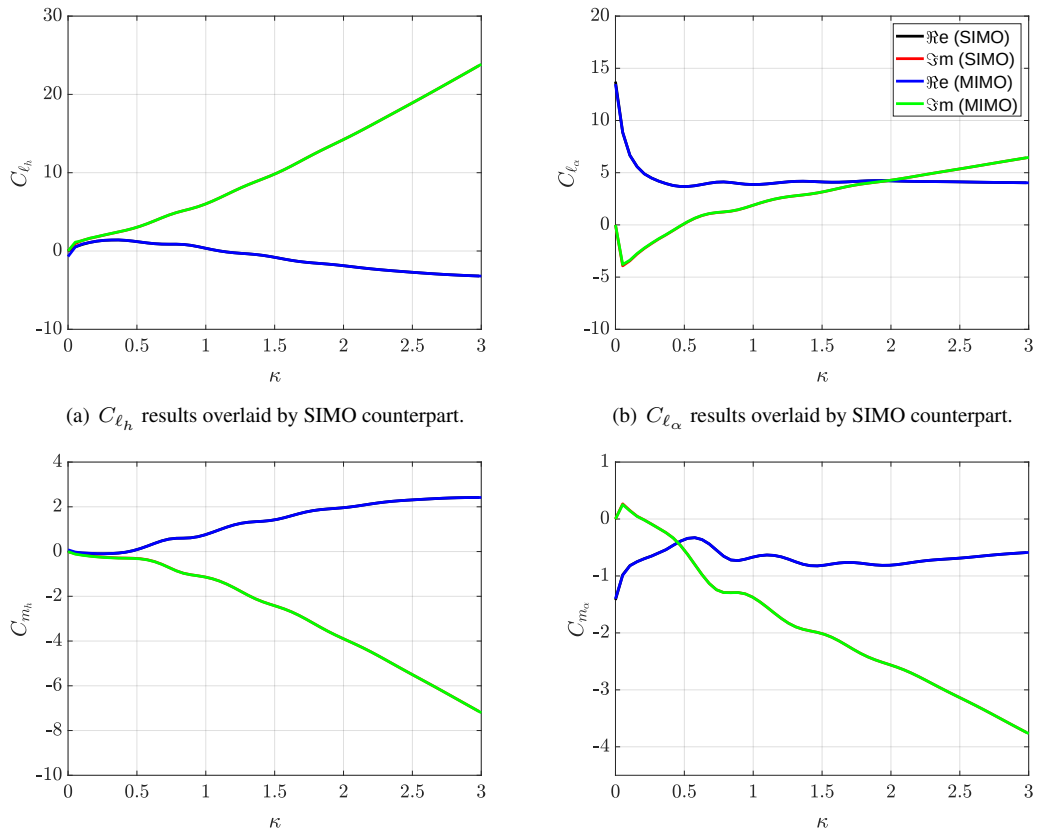

(a) C_{ℓ_h} results overlaid by SIMO counterpart.

(b) C_{ℓ_α} results overlaid by SIMO counterpart.

(c) C_{m_h} results overlaid by SIMO counterpart.

(d) C_{m_α} results overlaid by SIMO counterpart.

Figure 4. Aerodynamic transfer functions obtained using the SIMO and MIMO approaches.

calculated using the mode-by-mode, or SIMO, approach. However, when transforming the discrete aerodynamic time histories into frequency-domain transfer functions, one is faced with certain variables regarding the size of the sampled data and the number of overlapping points (Stoica *et al.*, 2005). To simplify the present analysis, the samples and overlaps were used in an integer value of information blocks. An information block is defined here by the length of the input discrete data where no variations occur.

The test case presented throughout this work is characterized by signal processing parameters based on four information blocks, one sample block, no overlapping blocks, and a rectangular window with the same size of the sampled data. The unsteady CFD results for this particular test case were obtained considering that the airfoil movement is prescribed by the orthogonal Walsh function inputs previously shown in Fig. 3. For comparison sake, there is also a test case related to the SIMO approach in which discrete step inputs are applied in each mode separately during the unsteady CFD simulations. A reason for including mode-by-mode analysis in the present work is that such approach has proven accuracy in literature to the extent that it composes the original ROM development process outlined by Silva (2008). Thus, the results obtained based on the SIMO approach are taken as benchmark in this work. Figure 4 shows that the resulting transfer functions for both plunge and pitch modes bear great resemblance to the benchmark SIMO case, indicating that the PSD-based procedure can effectively split the aerodynamic coefficient time histories into the contribution of each individual mode.

3.3 Rational-Function Approximation

The final stage in preparing data for frequency-domain aeroelastic stability analyses consists in representing the discrete data points of the aerodynamic transfer functions using rational-function approximations. The interpolating polynomials discussed in Subsec. 2.4 are applied for this purpose. Given that the accuracy of the approximation crucially depends on the values of the lag parameters β_n, these nonlinear parameters are selected by employing the simplex non-gradient optimization process proposed by Nelder and Mead (1965). When dealing with an optimization process, it is fundamental to ensure that the optimized poles, and the optimized linear coefficients by extension, that constitute the interpolating polynomial are independent of the initial pole set used to start the optimization. With this in mind, the optimization process is initially carried out several times for the same initial pole set in order to check whether the optimized poles depend on the numerical computations. In fact, it is observed that there are no discrepancies between the optimized pole sets for any computational run regardless of the interpolating polynomial used.

After confirming this independence, the optimized poles from distinct initial pole sets are finally investigated for a given RFA method. For comparison purposes, the same pole sets initiate the transfer function identification process using the first and second forms of Eversman and Tewari interpolating polynomials. In the second form of the polynomials, two or more poles of the approximation are represented by only one of them if they are very close to each other. In the present work, the difference between the poles must be below the threshold of 0.01 for them to be considered repeated poles. Two different initial pole sets are used in this work to initialize the simplex optimization process. All the initial pole set components are restricted in the closed interval between 0.25 and 1.2 in set A, whereas the initial pole set B is defined in the closed interval between 0.5 and 2.2. These restrictions take into account that the values for the lag parameters must be positive for the stability of the transfer functions, while the chosen magnitude span is based on the pole sets reported by Eversman and Tewari (1991). In addition to these restrictions, the initial poles are also equally spaced.

Tables 1-2 exhibits the resulting optimized lag parameters for the typical section problem when starting from the initial pole sets A and B, respectively, associated with both the first and second forms of Eversman and Tewari polynomials. In cases where repeated poles are identified according to the adopted threshold, the second form of the Eversman and Tewari polynomials indeed circumvents the repeated pole phenomenon. It should be noted that, although arising out of the phenomenon of repeated poles in the conventional first form method, Tabs. 1-2 show that the second form of the interpolating polynomials can be applied for even those cases in which repeated poles do not occur in the conventional approximation, yielding the same optimized lag parameters. More importantly, it is clear that the optimized lag parameters

Table 1. Optimized lag-parameter values initialized from the pole set A when considering both the first and second forms of Eversman and Tewari polynomials.

n_β	Lag parameters, β_n (First form)	Lag parameters, β_n (Second form)
1	3.584	3.584
2	0.079, 1.802	0.079, 1.802
3	0.026, 0.183, 1.612	0.026, 0.183, 1.612
4	0.040, 0.532, 0.532, 3.020	0.040, 0.537, 0.527, 3.018
5	0.032, 1.031, 0.610, 0.646, 0.609	0.032, 1.033, 0.623, 0.638, 0.611
6	0.035, 0.310, 0.393, 1.406, 0.448, 0.501	0.036, 0.371, 0.517, 0.527, 0.480, 1.109

Table 2. Optimized lag-parameter values initialized from the pole set B when considering both the first and second forms of Eversman and Tewari polynomials.

n_β	Lag parameters, β_n (First form)	Lag parameters, β_n (Second form)
1	3.584	3.584
2	0.079, 1.802	0.079, 1.802
3	0.078, 1.702, 28.584	0.078, 1.702, 28.584
4	0.040, 0.532, 0.532, 3.018	0.040, 0.527, 0.537, 3.018
5	0.032, 0.431, 2.273, 0.432, 0.427	0.032, 0.459, 1.967, 0.448, 0.469
6	0.032, 0.443, 4.103, 0.451, 0.451, 2.603	0.032, 0.479, 0.489, 1.958, 0.469, 3.246

for a given RFA method are significantly different depending on the pole set initially assumed. This behavior is particularly relevant because the frequency-domain aeroelastic stability analysis is based on data from the approximated aerodynamic transfer functions, characterized by the lag parameters and the corresponding linear coefficients.

Once the RFA coefficients are computed, one can verify the fitting accuracy by comparing the original CFD data with the resulting polynomial fit. The data fitting is performed up to the reduced frequency $\kappa = 3$ because the flutter phenomenon typically occurs in the low reduced frequency portion of the frequency spectrum generated by the CFD simulation. Figure 5 depicts the aerodynamic transfer functions obtained directly from CFD data using the MIMO approach, and the resulting rational-function approximation. As one can see in Fig. 5, the polynomial fitting seems to produce a reasonable approximate curve to replace the CFD data. Discrepancies, however, mainly occur in regions in which there is a rapid variation in the CFD results, in these regions the interpolated RFAs do not seem to be able to completely follow the original transfer function. Moreover, the coefficients due to the motion in α seem to be particularly affected by the approximation inherent to the RFA calculation process.

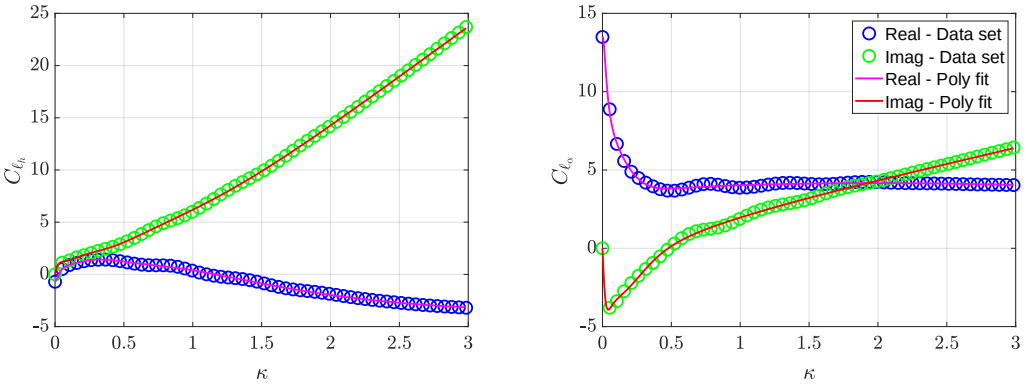

(a) C_{ℓ_h} coefficient.

(b) C_{ℓ_α} coefficient.

(c) C_{m_h} coefficient.

(d) C_{m_α} coefficient.

Figure 5. Aerodynamic transfer functions considering 6 optimized poles, obtained from the initial pole set A, using the second form of Eversman and Tewari polynomials.

3.4 Aeroelastic Stability Analysis

Finally, the approximated polynomials are employed in the solution of the flutter stability eigenvalue problem. The stability root loci of the structural modes generated from the second form of the interpolating polynomials can be seen in Fig. 6. This figure also presents numerical results from the mode-by-mode step excitation that refers to the SIMO approach, and literature data extracted from the work of Rausch *et al.* (1990). In the search for the flutter onset point, the characteristic dynamic pressure parameter Q^* is varied from 0.1 up to 1.0 in $\Delta Q^* = 0.01$ intervals. Obviously, not all the calculated eigenvalues are indicated in the figure in order to avoid cluttering it. However, the values shown for the present calculations allow for a visual indication of the flutter instability condition. The literature data, however, are only available for $Q^* = 0.2$, 0.5, and 0.8.

By definition, the flutter onset point is identified as the point at which the damping of one of the aeroelastic modes becomes identically zero. In other words, the flutter onset point is given by the characteristic speed at which each specific root locus crosses to the right half of the complex plane. In cases where the flutter onset point was not readily available, however, the instability onset point was computed based on the quadratic interpolation of the two closest damping values at the stability frontier $\sigma_1/\omega_r = 0$. The resulting root locus for the first structural mode, shown in Fig. 6(a), presents an aeroelastic instability as the roots cross to the right half of the complex plane with increasing dynamic pressure. On the other hand, in the second structural mode, the roots remain on the left half of the complex plane, as expected. These results also show that the modal damping, σ, and frequency, ω, behavior of the aeroelastic modes predicted using the mode-by-mode step excitation and the Walsh functions are very similar, indicating that these procedures are essentially equivalent concerning the aeroelastic instability identification. Nevertheless, it is important to remind that the MIMO approach offers significant computational time savings over the SIMO counterpart.

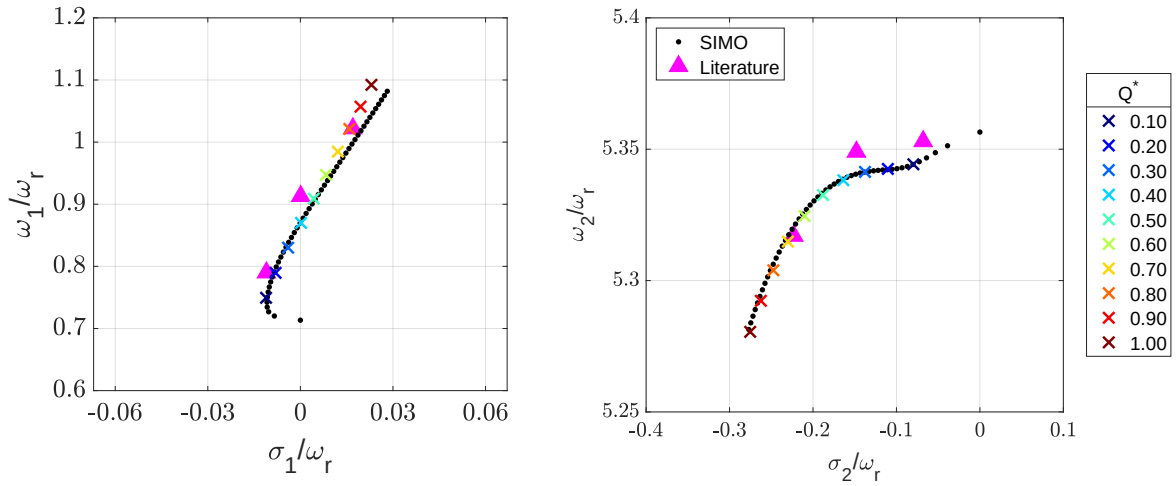

(a) First structural mode.

(b) Second structural mode.

Figure 6. Root locus considering 6 optimized poles, obtained from the initial pole set A, using the second form of Eversman and Tewari polynomials.

Tables 3-6 present the modal damping and frequency values at the flutter onset point for both structural modes. In particular, Tables 3-4 consider the optimized poles from Tab. 1 to compose the first and second forms of RFAs of the aerodynamic transfer functions, respectively. Similarly, Tables 5-6 consider the optimized poles from Tab. 2 to respectively compose the first and second forms of RFAs. The right-most column of Tables 3-6 presents the percentage error comparing the flutter characteristic speeds U_f^* obtained using RFA-based ROMs, and the numerical data from Rausch *et al.* (1990) for the same flight condition. Rausch *et al.* (1990) state that flutter occurs close to $Q^* = 0.5$, which is a near neutrally stable condition, for the same typical section configuration. It corresponds to a reference characteristic speed of $U^* = 5.4772$.

As previously observed in Tabs. 1-2, one can see that repeated poles are only encountered when assuming more than three augmented poles for this particular test case. In these cases, Tables 3-4 indicate that using the second form of the interpolating polynomials brings the flutter onset point results slightly closer to the reference value compared to using the first form. As an example, by replacing the first form of the interpolating polynomials with the second form, the percentage error of this test case with $n_\beta = 6$ reduces from 11.2% to 11.1%. The reason for this behavior is that the second form of the polynomials is designed to fine tune the optimized poles in areas where repeated poles cause discontinuities. Moreover, note that, regardless of the initial pole set and RFA formulation, the reduced-order models composed by a single augmented state, $n_\beta = 1$, yield percentage errors of the flutter onset point as high as 99%. This is

possibly due to limited flexibility in the pole positioning.

Another aspect to notice is that distinct optimized poles can yield different flutter onset points. Consider, for instance, the optimized pole sets for $n_\beta = 3$ and the first form of the polynomials, shown in Tabs. 1-2. It is clear that, for the same total number of poles and RFA formulation, these optimized poles are considerably different in magnitude from each other. An evidence of this is the fact that the maximum magnitudes in these optimized pole sets are approximately 1.6 and 28.6 when initializing the optimization process with pole sets A and B, respectively. As a consequence, Tabs. 3 and 5 show that these distinct optimized poles result in flutter onset points of 6.85 and 4.66, described in terms of the characteristic speed. The same behavior is observed when considering the second form of the interpolating polynomials.

Table 3. Flutter onset points for NACA 0012 airfoil at $M_\infty = 0.80$ with up to 6 optimized poles, initialized from the pole set A, using the first form of Eversman and Tewari polynomials.

n_β	σ_1/ω_r	ω_1/ω_r	σ_2/ω_r	ω_2/ω_r	Q_f^*	U_f^*	Error %
1	1.8×10^{-5}	0.106	-0.0001	0.092	0.100	0.04	99.3
2	-1.2×10^{-8}	0.869	-0.158	5.333	0.400	4.87	11.1
3	-9.3×10^{-12}	1.018	-0.226	5.318	0.791	6.85	25.1
4	-4.5×10^{-10}	0.907	-0.182	5.331	0.500	5.47	0.05
5	-2.5×10^{-10}	0.891	-0.176	5.334	0.445	5.17	5.7
6	-6.9×10^{-9}	0.867	-0.163	5.338	0.400	4.86	11.2

Table 4. Flutter onset points for NACA 0012 airfoil at $M_\infty = 0.80$ with up to 6 optimized poles, initialized from the pole set A, using the second form of Eversman and Tewari polynomials.

n_β	σ_1/ω_r	ω_1/ω_r	σ_2/ω_r	ω_2/ω_r	Q_f^*	U_f^*	Error %
1	1.8×10^{-5}	0.106	-0.0001	0.092	0.100	0.04	99.3
2	-1.2×10^{-8}	0.869	-0.158	6.687	0.400	4.87	11.1
3	-9.3×10^{-12}	1.018	-0.226	5.451	0.791	6.85	25.1
4	-3.6×10^{-11}	0.907	-0.182	5.356	0.500	5.48	0.004
5	-4.7×10^{-10}	0.891	-0.177	5.651	0.455	5.17	5.6
6	-6.6×10^{-9}	0.868	-0.163	6.684	0.400	4.87	11.1

Table 5. Flutter onset points for NACA 0012 airfoil at $M_\infty = 0.80$ with up to 6 optimized poles, initialized from the pole set B, using the first form of Eversman and Tewari polynomials.

n_β	σ_1/ω_r	ω_1/ω_r	σ_2/ω_r	ω_2/ω_r	Q_f^*	U_f^*	Error %
1	1.8×10^{-5}	0.106	-0.0001	0.092	0.100	0.04	99.3
2	-1.2×10^{-8}	0.869	-0.158	5.333	0.400	4.87	11.1
3	-5.7×10^{-9}	0.852	-0.150	5.335	0.364	4.66	14.8
4	-6.0×10^{-10}	0.907	-0.182	5.331	0.500	5.47	0.07
5	-1.2×10^{-9}	0.863	-0.160	5.337	0.381	4.78	12.7
6	-3.8×10^{-10}	0.859	-0.158	5.338	0.373	4.73	13.7

Table 6. Flutter onset points for NACA 0012 airfoil at $M_\infty = 0.80$ with up to 6 optimized poles, initialized from the pole set B, using the second form of Eversman and Tewari polynomials.

n_β	σ_1/ω_r	ω_1/ω_r	σ_2/ω_r	ω_2/ω_r	Q_f^*	U_f^*	Error %
1	1.8×10^{-5}	0.106	-0.0001	0.092	0.100	0.039	99.3
2	-1.2×10^{-8}	0.869	-0.158	6.687	0.400	4.87	11.1
3	-5.7×10^{-9}	0.852	-0.150	5.860	0.364	4.66	14.8
4	-2.8×10^{-11}	0.907	-0.182	5.342	0.509	5.48	0.002
5	-2.9×10^{-9}	0.866	-0.161	6.694	0.391	4.81	12.1
6	-4.0×10^{-10}	0.860	-0.158	5.484	0.382	4.73	13.6

4. CONCLUDING REMARKS

The effects of rational-function approximation (RFA) coefficients that compose the aerodynamic transfer functions on transonic aeroelastic stability analyses are assessed. Regardless of the RFA formulation investigated in this work, the optimized poles obtained from multiple computational runs starting with the same initial pole set show no variations. However, it is evident that, depending on the initial pole values, the optimization process can converge to different poles and, consequently, to distinct flutter onset points for a given flight condition. It means that, if an alternative initial pole set is used, the flutter onset results can exhibit significant variations, either converging or diverging from the reference data. This dependence is possibly attributed to the presence of multiple local minima in the cost function being minimized during the optimization process. This is because, while the Nelder-Mead optimization algorithm converges to a local minimum, it does not ensure the identification of a global minimum. It is true that, despite the difficulties regarding the optimization process, the RFA-based aerodynamic ROM can attain remarkably low percentage errors as minimal as 0.002% compared to the numerical benchmark, especially associated with the second form of the Eversman and Tewari polynomials.

5. ACKNOWLEDGMENTS

The authors gratefully acknowledge the support provided by Fundação de Amparo à Pesquisa do Estado de São Paulo, FAPESP, through a Master of Science Scholarship for the first author (FAPESP Process No. 2022/01397-0), and also under the Research Grant No. 2013/07375-0. This work was also supported by Fundação Coordenação de Aperfeiçoamento de Pessoal de Nível Superior, CAPES, under the Research Grants No. 88887.634461/2021-00 and 88887.609895/2021-00. The present work has also received support from Conselho Nacional de Desenvolvimento Científico e Tecnológico, CNPq, under the Research Grant No. 309985/2013-7.

6. REFERENCES

Azevedo, J.H.F., Azevedo, J.L.F. and Silva, R.G.A., 2013. "Effects of the Aerodynamic Data in a MIMO System Identification Framework for Aeroelastic Analyses". AIAA Paper No. 2013-1486, *54th AIAA/ASME/ASCE/AHS/ASC Structures, Structural Dynamics, and Materials Conference*, Boston, MA. DOI 10.2514/6.2013-1486.

Bisplinghoff, R.L., Ashley, H. and Halfman, R.L., 1955. *Aeroelasticity*. Addison-Wesley Publishing Company, Inc.

Eversman, W. and Tewari, A., 1991. "Consistent Rational-Function Approximation for Unsteady Aerodynamics". *Journal of Aircraft*, Vol. 28, No. 9, pp. 545–552. DOI 10.2514/3.46062.

Marques, A.N. and Azevedo, J.L.F., 2008. "Numerical Calculation of Impulsive and Indicial Aerodynamic Responses Using Computational Aerodynamics Techniques". *Journal of Aircraft*, Vol. 45, No. 4, pp. 1112–1135. DOI 10.2514/1.32151.

Nelder, J.A. and Mead, R., 1965. "A Simplex Method for Function Minimization". *The Computer Journal*, Vol. 7, No. 4, pp. 308–313. ISSN 0010-4620. DOI 10.1093/comjnl/7.4.308.

Rausch, R.D., Batina, J.T. and Yang, H.T.Y., 1990. "Euler Flutter Analysis of Airfoils Using Unstructured Dynamic Meshes". *Journal of Aircraft*, Vol. 27, No. 5, pp. 436–443. DOI 10.2514/3.25295.

Silva, W.A., 2018. "AEROM: NASA's Unsteady Aerodynamic and Aeroelastic Reduced-Order Modeling Software". *Aerospace*, Vol. 5, No. 2, p. 41.

Silva, W. and Bartels, R.E., 2004. "Development of Reduced-Order Models for Aeroelastic Analysis and Flutter Prediction Using the CFL3Dv6.0 Code". *Journal of Fluids and Structures*, Vol. 19, No. 6, pp. 729–745. ISSN 0889-9746. DOI 10.1016/j.jfluidstructs.2004.03.004.

Silva, W.A., 2008. "Simultaneous Excitation of Multiple-Input/Multiple-Output CFD-Based Unsteady Aerodynamic Systems". *Journal of Aircraft*, Vol. 45, No. 4, pp. 1267–1274. DOI 10.2514/1.34328.

Silva, W.A., Vatsa, V.N. and Biedron, R.T., 2009. "Development of Unsteady Aerodynamic and Aeroelastic Reduced-Order Models Using the FUN3D Code". *IFASD Paper 2009–030*.

Stoica, P., Moses, R.L. *et al.*, 2005. *Spectral Analysis of Signals*, Vol. 452. Pearson Prentice Hall, Upper Saddle River, NJ.

Thomas, J.P. and Dowell, E.H., 2019. "Discrete Adjoint Approach for Nonlinear Unsteady Aeroelastic Design Optimization". *AIAA Journal*, Vol. 57, No. 10, pp. 4368–4376. DOI 10.2514/1.J057504.

Tiffany, S.H. and Adams, W.M., 1988. "Nonlinear Programming Extensions to Rational Function Approximations of Unsteady Aerodynamics". Technical Report NASA–TP–2776, NASA.

7. RESPONSIBILITY NOTICE

The authors are solely responsible for the printed material included in this paper.